Arch. Metall. Mater. **66** (2021), 2, 437-442

DOI: 10.24425/amm.2021.135876

R.L.P. TEIXEIRA[1*], J.C. DE LACERDA[1], I.C. CONCEIÇÃO[1],
S.N. DA SILVA[2], G.O. SIQUEIRA[1], F. MOURA FILHO[1]

THE EFFECTS OF NIOBIUM ON THE BIOACTIVITY OF Ni-Ti-Al-Nb SHAPE MEMORY ALLOYS

This work aims to analyze the effects of niobium on the bioactivity of a titanium, nickel, aluminum, and niobium alloy obtained by the Plasma Skull Push Pull process (PSPP). Titanium alloys, such as NiTinol (NiTi), are metallic biomaterials that have wide application in health and surgical prostheses. In this work the microstructural and bioactivity characteristics of the alloys are evaluated. The addition of aluminum improves alloy ductility and reduces its cost. The addition of niobium favors the hydroxyapatite nucleation. Therefore, the addition of the combination of the two elements contributes to lower cost and better alloy bioactivity.

Keywords: nitinol, niobium, aluminum, bioactivity, cytotoxicity

1. Introduction

Biomaterials differ from other materials in that they contain a combination of mechanical, chemical, physical, and biological properties that make them applicable in prostheses and implants. Implants are widely applied in health treatments for organ function recovery. According to the literature, there is a prediction of a substantial increase in the use of implants in orthopedic surgeries in the coming years [1-2].

The use of biomaterials in the human body began in the 19th century with the use of natural materials in such prostheses as a wooden leg and ivory denture, among others. Vanadium and titanium began to be applied in prostheses in the 1930s. Over time these metals began to exhibit problems of biocompatibility and corrosion resistance in certain applications. Due to this, they have been replaced by stainless steel alloys and cobalt-based alloys [3].

Shape memory alloys were discovered in 1960 and introduced into biomechanics in 1973. These alloys have application in orthodontics and temporary fixation of the spine and long bones, despite their low modulus of elasticity (from 30 MPa to 50 MPa) compared to stainless steels [3]. Another important aspect to be considered in terms of mechanical properties of shape memory alloys is related to their fatigue limit and yield limit [4].

Currently, the metals most used in implants are stainless steels, chromium-cobalt alloys, and titanium alloys. These alloys have biocompatibility as well as good toughness. It must be considered that the cobalt-based alloys present limitations for their application in hip joint implantation. In this case, friction and corrosion wear may lead to implant loosening, compromising its performance [3].

Titanium and its alloys are widely used in implants due to their biocompatibility, corrosion resistance, mechanical properties, and bioadhesion characteristics. Eventually, titanium implants can cause fractures and wear on hard tissue (bone) as well as joint surfaces [1].

Shape memory alloys (SMA) are functional metallic materials that can recover from large pseudoplastic deformations when subjected to mechanical loading and/or heating. The SMA is widely applied in the aerospace, automotive, and telecommunications industries, as well as in medical and dental applications (orthodontic wires, stents, and orthopedic prostheses) [5-7].

The shape memory effect is related to phase transformations: authenite-martensite. At low temperature the martensite presents little symmetrical crystalline structure and at high temperature the austenite presents symmetrical crystalline structure. Thus, with temperature changes, the SMA can transform from martensite to austenite or austenite to martensite: With heating the martensite turns into austenite and with cooling the opposite happens. These transformations are the key to the SMA form return process called SMF [8]. Among the SMAs, there is NiTinol. This alloy consists of titanium and nickel in

[1] UNIVERSIDADE FEDERAL DE ITAJUBÁ, ITABIRA, MG, BRAZIL
[2] CENTRO FEDERAL DE EDUCAÇÃO TECNOLÓGICA DE MINAS GERAIS, BELO HORIZONTE, MG, BRAZIL
* Corresponding author: ricardo.luiz@unifei.edu.br

equiatomic compositions. This alloy has wide application and presents biocompatibility of interest in surgical prostheses and orthodontic wires [9].

NiTinol alloy is a SMA that the shape memory effect can be affected either by the process parameters or the compositional and microstructural variability. without the need for direct, cumbersome measurements. The transformation temperatures in NiTinol alloy are sensitive to Ni content in the Ni-rich side of the stoichiometry, as well as the precipitate structure and grain size. The addition of niobium is known for raising the characteristic temperatures of martensitic transformation while aluminum lowers. The addition of aluminum to the NiTinol may produce a lower density alloy. Thus, small differences in composition and microstructure therefore result in large differences in the transformation temperatures. This feature makes the alloy more suitable for leg bone implants and hand prosthesis applications. Furthermore, the addition of aluminum reduces the cost and can be considered non-toxic according to the proposal presented in this paper [10,11].

Aiming for new alternatives to SMAs, in the present work, a NiTinol type memory alloy with the addition of aluminum and niobium as alloying elements is studied. These elements aim to stabilize austenite and martensite, respectively. Plasma Skull Push Pull (PSPP) process casting was used [12-13]. Niobium addition still aims to stabilize the titanium alpha phase in NiTinol and improve hydroxyapatite nucleation [14-16].

2. Experimental procedures

For the experiments, industrial orthodontic NiTinol wire was used. The NiTinol wire was melted by the PSPP (EDG oven, Discovery model) process with the addition of niobium and aluminum in the proportions indicated in Table 1. In the PSPP, argon was used for plasma production.

TABLE 1

Ni-Ti-Al-Nb shape memory alloys

	Sample 1		Sample 2		Sample 3	
	g	mol	g	mol	g	mol
NiTi	2.0000	0.0188	2.0000	0.0188	2.0000	0.0188
Al	—	—	2.0000	0.0741	2.0000	0.0741
Nb	—	—	0.5000	0.0054	1.0000	0.0108

Table 1 presents 3 alloy formulations, produced in 3 samples (Sample 1, Sample 2, and Sample 3). Initially, the samples were subjected to attack in 5M NaOH solution at 60°C for 24 hours. This first attack aimed to produce hydroxyl on the alloy surface. Thus, deposition of hydroxyapatite and other calcium phosphates was facilitated. After this first stage, the samples were immersed in a simulated body fluid (SBF). The SBF chemical composition is shown in Table 2. The SBF was prepared by dissolving NaCl, KCl, $NaHCO_3$, $MgCl_2 \cdot 6H_2O$, $CaCl_2$, and KH_2PO_4 in distilled water and buffered at pH = 7.25 with TRIS (tris-hydroxymethylaminomethane) and HCl 1M at 37°C [17]. The calcium phosphate coating obtained in the samples was analyzed morphologically by scanning electron microscopy (SEM), crystallographically by X-ray diffraction (DRX), and cytotoxicity by growth of bacterium according to the NCCLS M2-A8 standard [18]. The diffractograms were performed with fast and long scanning at the diffraction angle (2θ) from 30° to 120° in steps of 0.02° with 0.25 seconds per step. The diffraction peaks were identified based on the Diffraction Archives of the International Center for Diffraction Data (ICDD) [19].

The toxicity tests using bacterium were developed based on inhibition of growth, oxygen consumption, colony formation, morbidity, bioluminescence, and genotoxicity [20-21]. Sample 1, Sample 2, and Sample 3 were suitably autoclaved at 121°C for 20 min. For the analytical procedure an initial dilution of 1:10 was made with 5 hour incubation. The dilution was performed for the three bacteria recommended by ANVISA (National Health Surveillance Agency - Brazil): *Staphylococcus aureus, Escherichia coli,* and *Candida albicans.* For the cytotoxicity tests, the samples were placed, respectively, in three Petri dishes containing the culture media already inoculated with the microorganisms: *Staphylococcus aureus, Escherichia coli,* and *Candida albicans*. The bacterium *Candida albicans* was inoculated with a dilution of 1:10 after 5 hours of incubation. The bacteria *Staphylococcus aureus* and *Escherichia coli* were inoculated for 5 hours with subsequent dilution in the ratio of 1:40. Using a sterile swab, the bacteria were applied twice consecutively on the three respective plates (Sample 1: *Candida albicans*; Sample 2: *Staphylococcus aureus*; Sample 3: *Escherichia coli*). Plates were maintained for 18 hours at 35°C. After application, the bacterium *Candida albicans* was immersed twice in Sabouraud medium. The bacteria *Staphylococcus aureus* and *Escherichia coli* were also immersed twice, but in Miller Hinton medium. After 18 hours of incubation, a visual and qualitative analysis of the bacteria growth process in each of the Petri dishes was carried out, according to the recommendation of IS0 10993-5 [22].

TABLE 2

Concentration of SBF and Human Blood Plasma

Ions	Na^+	K^+	Mg^{2+}	Ca^{2+}	Cl^-	HCO^{3-}	$HPO4^{2-}$	$SO4^{2-}$
SBF(mM)	142.0	5.0	1.5	2.5	147.8	4.2	1.0	0.5
Human Blood Plasma	142.0	5.0	1.5	2.5	103.0	27.0	1.0	0.5

SEM (TESCAN, model VEGA3 BS) was used for morphological characterization of the surface coating. The semi-quantitative chemical analyses of the samples were performed by energy-dispersive X-ray spectroscopy (EDS Bruker). All samples were previously covered with 250 Angstroms of conductive gold-palladium alloy vacuum-evaporated (PVD) to provide a suitable microanalysis. Surface roughness and thickness of samples were measured with stylus roughness Sloan DekTak II surface profilometer (Dektak, Veeco Instruments Inc., Plainview, NY, USA) [23].

3. Results and discussion

The increase of the niobium content lowers the martensite-austenite transformation temperature [16]. Samples 2 and 3 were harder than Sample 1 (Sample 1: 302 ± 5 HV; Sample 2: 489 ± 32 HV; and Sample 3: 588 ± 54 HV). Vickers microhardness tests were performed at 2.0 Newtons for 10 seconds. The increase of the microhardness in Samples 2 and 3 compared to Sample 1 can be attributed to the presence of niobium, which is a stabilizer of the beta phase of titanium [22,24,25].

According to Figure 1(a), Sample 1 shows less roughness indicating homogeneous melting during alloy production. As can be seen in Figure 1(b), Sample 2 shows greater roughness after the solidification of the alloy due to the presence of dispersed aluminum precipitates. Apparently, the precipitates did not adequately melt during the alloying process. Figure 2 shows the chemical composition of the specimens obtained by EDS analysis. In Figure 1(c), in Sample 3, the occurrence of roughness was observed due to the existence of dispersed aluminum precipitates and inhomogeneous melting. In this case there was less roughness compared to Sample 2.

The phases present in the produced alloy were identified by X-ray diffraction, as shown in Figure 3. Sample 1 (Nitinol) showed well-defined diffraction peaks at (110) and (211) for austenite and at (202) for martensite [26,27]. Sample 2 (Nitinol, Al, Nb) also showed the same peaks as Sample 1, but with greater intensity. This higher intensity of the diffraction peaks can be attributed to the overlap of signals between the aluminum and titanium. Sample 3 showed the same peaks as Sample 1 and Sample 2, and a new austenite peak (220). This new austenite peak may be correlated with increasing niobium, which stabilizes and intensifies the austenitic phase, β [26,27].

As shown in Figure 4, the presence of niobium acts as a nucleating agent for hydroxyapatite on the surface during deposition by autocatalysis [28,29]. It can also be observed in Figure 4 that the increase of niobium in the composition (Sample 2 and Sample 3) caused the appearance of new crystals of

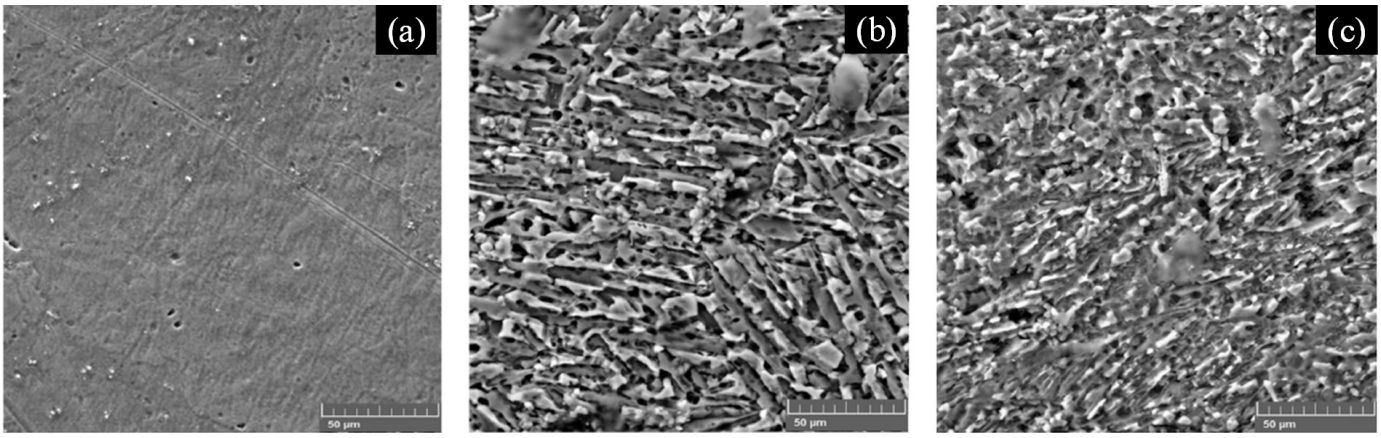

Fig. 1. Ni-Ti-Al-Nb shape memory alloys: (a) Sample 1; (b) Sample 2; (c) Sample 3. SEM

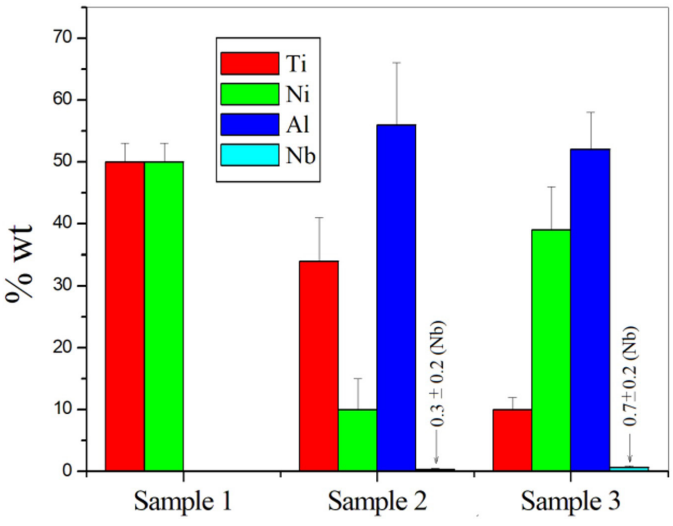

Fig. 2. Chemical composition of samples. EDS

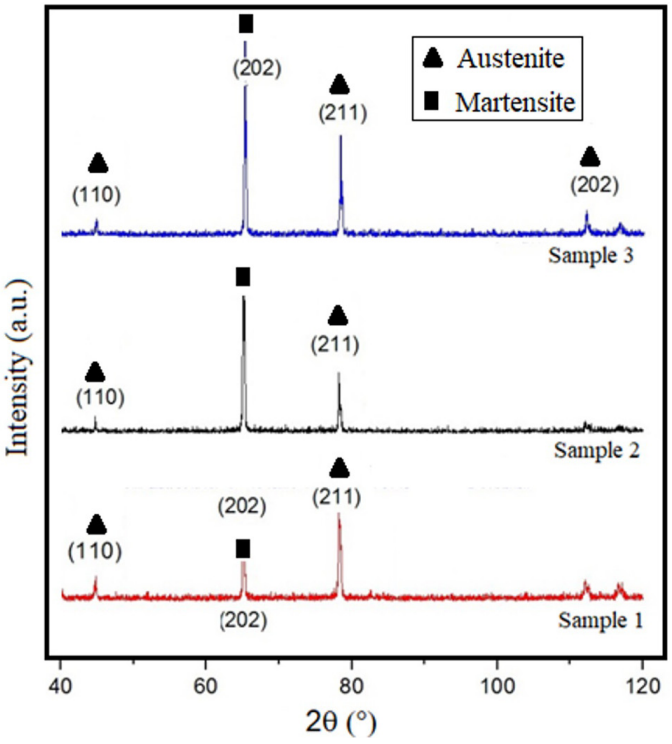

Fig. 3. Sample 1, Sample 2, and Sample 3 diffractograms

hydroxyapatite with different crystallographic orientations. The increase of hydroxyapatite contributes to better calcification in vivo of the samples [30].

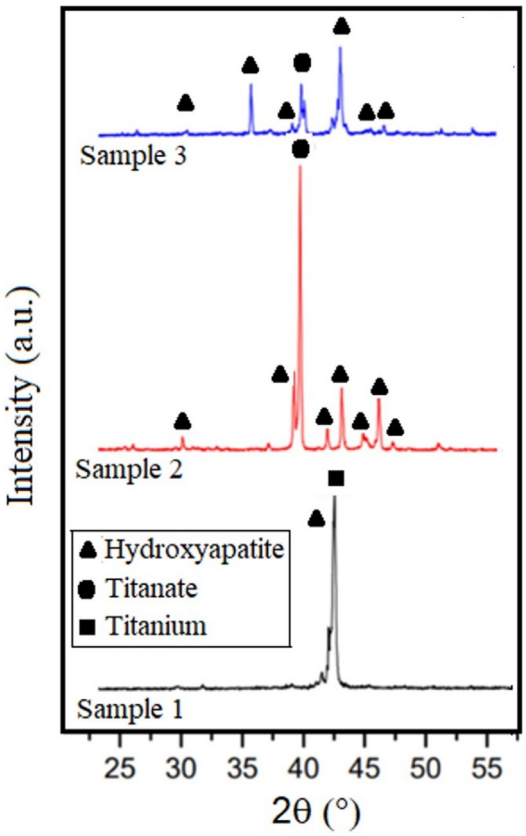

Fig. 4. Diffractograms: Samples after immersion in SBF solution

The presence of agglomerated hydroxyapatite on the surface of NiTinol (Sample 1) can be observed in Figure 5. The presence of P, Ca, and O in the hydroxyapatite region was identified by EDS analysis (Table 3). A small difference in the Ca/P ratio was observed in Sample 3 in relation to Sample 2. This difference can be attributed to its higher niobium content. The higher niobium content usually results in higher nucleation and thickness of hydroxyapatite [28,29].

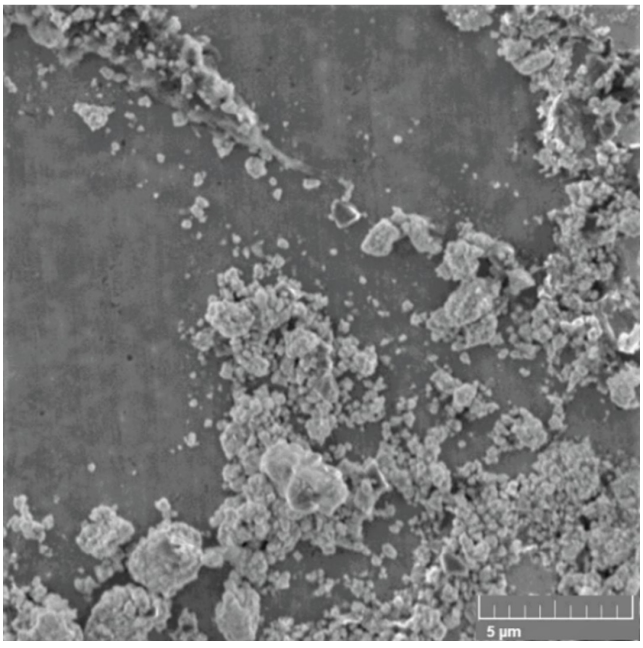

Fig. 5. Hydroxyapatite on Sample 1. SEM

In Figure 6, the presence of agglomerated hydroxyapatite on the surface of Sample 2 (Nitinol, Al, Nb) can be observed. The presence of P, Ca, and O was identified in the hydroxyapatite region (Table 3), but with less intensity than in Sample 1 (Nitinol).

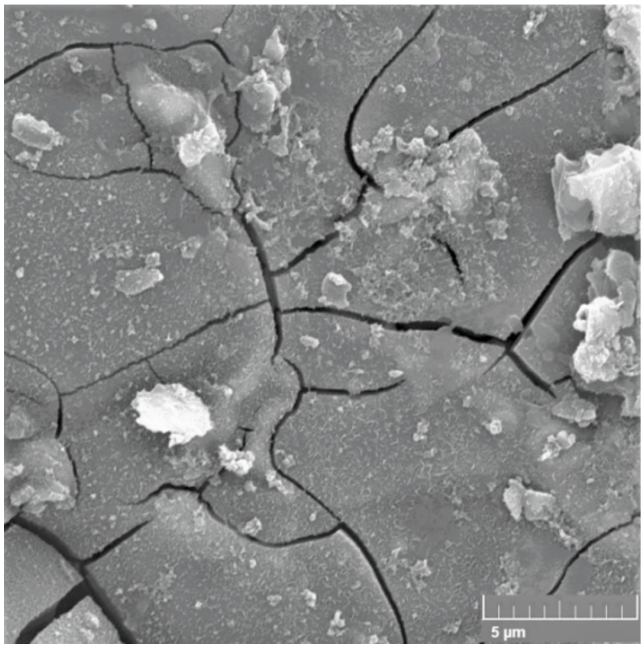

Fig. 6. Hydroxyapatite on Sample 2. SEM

The morphology of plates formed on the surface of Sample 2, presented in Figure 6, occurred due to autocatalysis hydroxyapatite formation with greater surface roughness (Fig. 1b). The cracks observed in Figure 6 can be attributed to the residual tensile stresses generated on the hydroxyapatite. The residual tensile stresses occurred due to the combination of high adhesion on the rough surface of the substrate and its consequent contraction during the drying process. An illustration of the formation mechanism of hydroxyapatite fractured plates is shown in Figure 7.

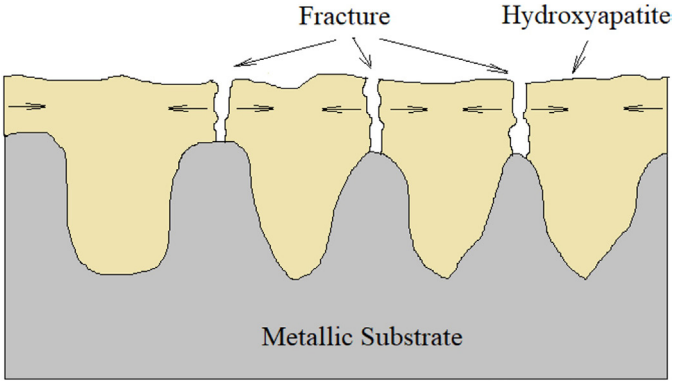

Fig. 7. Formation mechanism of hydroxyapatite fractured plates

In Figure 8 the presence of agglomerated hydroxyapatite on the surface of Sample 3 (Nitinol, Al, Nb) can be observed. In Sample 3 no fractures were observed on plates similar to those in Sample 2. The absence of the mentioned fractures can be attributed to the formation of thicker hydroxyapatite film. Greater thickness implies less roughness. In Figure 8 fractures of the hydroxyapatite layer can be seen in the pore regions occurring due to the residual tensile stresses generated during their drying on the substrate.

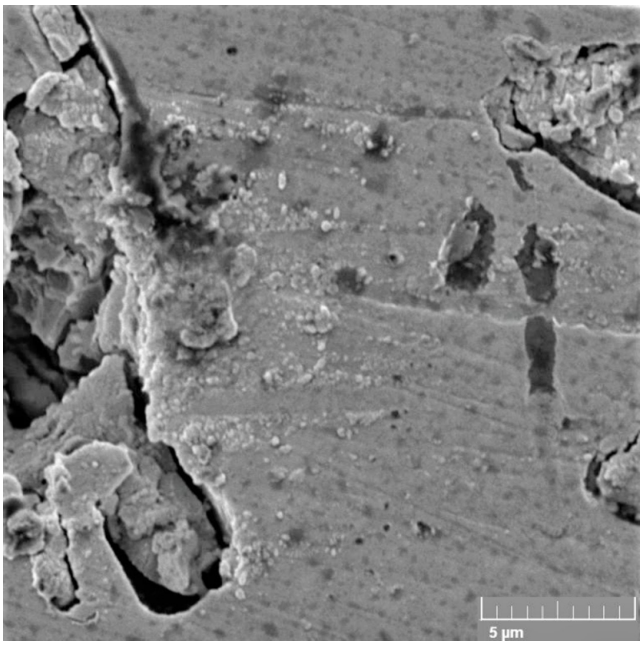

Fig. 8. Hydroxyapatite on Sample 3. SEM

The Ca/P ratio shown in Table 3 is indicative of amorphous hydroxyapatite formation [31-33]. Formation of amorphous hydroxyapatite is not confirmed in this work by the X-ray diffraction results shown in Figure 4.

Results of bacterial growth (*Candida albicans, Staphylococcus aureus,* and *Escherichia coli*) in the three samples are shown in Figure 9. As the growth of bacteria in all of them has been verified, they can be considered non-cytotoxic; that is, they do not present toxicity to the cells.

TABLE 3

Chemical composition of coating

Elements	Chemical Composition (atomic %)		
	Sample 1	Sample 2	Sample 3
P	9.6	2.4	2.8
Ca	9.4	1.5	1.9
O	69.8	29.0	30.2
Ti	5.3	11.2	8.1
Ni	1.3	25.1	2.8
Al	—	4.3	23.2
Nb	—	9.2	2.0
Ca/P	0.98	0.63	0.68

The cytotoxicity results of Samples 1, 2, and 3 presented in Figure 9 indicate the application biocompatibility of the alloys in hard tissue implants in living beings. In this case, the addition of niobium and aluminum apparently did not make alloys (Sample 2 and Sample 3) toxic in applications to living things. It was also observed that a higher content of niobium (Sample 3) can produce a layer of hydroxyapatite (bioactivity) with greater thickness due to its nucleating effect (Fig. 8).

3. Conclusions

- Higher martensite stabilization by the addition of niobium in Sample 2 and 3 caused modification in the microstructure and consequent increase in the Vickers microhardness of the alloys compared to the NiTinol sample;
- The presence of niobium and aluminum in the Sample 2 and 3 alloys during the solidification process after plasma fusion caused a change in the microstructure and surface morphology of the alloys compared to the Sample 1 alloy, making them rougher;
- The highest roughness produced in Sample 2 alloy is associated with the thin layer of hydroxyapatite resulting in a fragile surface fractures appearance;
- In Sample 2 alloy, the appearance of fragile surface fractures due to residual tensile stresses generated in the deposited hydroxyapatite layer is associated with the thin deposited hydroxyapatite layer;

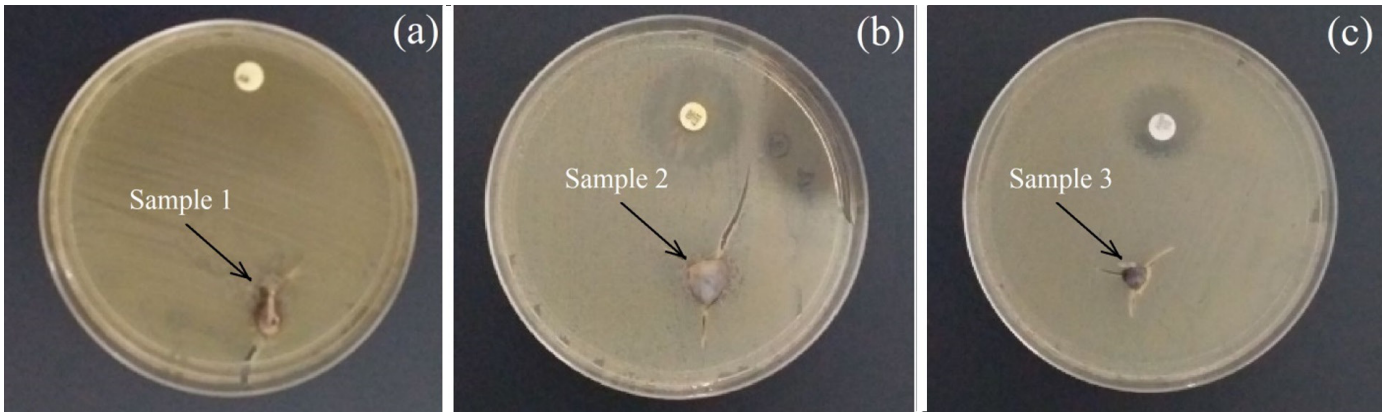

Fig. 9. Growth of bacteria: (a) Sample 1 – Candida albicans; (b) Sample 2 – Staphylococcus aureus; (c) Sample 3 – Escherichia coli

- In the Sample 3 alloy with higher niobium content, there was a thicker hydroxyapatite layer;
- The decrease in the intensity of residual tensile stresses is according to the smaller amount of fragile fracture regions that occurred in the Sample 3 alloy;
- The addition of niobium and aluminum (Samples 2 and 3) apparently did not affect the biocompatibility and bioactivity behavior of the alloys compared to NiTinol alloy (Sample 1).

Acknowledgements

The authors would like to acknowledge the Foundation for Research Support of the State of Minas Gerais (FAPEMIG), the Federal University of Itajubá (UNIFEI) – Itabira Campus, the Federal Center of Technological Education of Minas Gerais – CEFET-MG for the availability of laboratory technical resources and the Metals Group from UNIFEI, Itabira Campus.

REFERENCES

[1] Y. Kirmanidou, M. Sidira, M. E. Drosou, V. Bennani, A. Bakopoulou, A. Tsouknidas, K. Michalakis, Biomed Res. Int. **2016**, 2908570 (2016) pages. DOI: http://dx.doi.org/10.1155/2016/2908570

[2] G.A. Longhitano, M.A. Larosa, A.L.J. Munhoz, C.A.C. Zavaglia, M.C.F. Ierardi, Mater. Res-Ibero-Am. J. **18**, 838-842 (2015). DOI: http://dx.doi.org/10.1590/1516-1439.014415

[3] L. Kunčická, R. Kocich, T.C. Lowe, Prog. Mater. Sci. **88**, 232-280 (2017). DOI: https://doi.org/10.1016/j.pmatsci.2017.04.002

[4] J.R. Davis, Handbook of materials for medical devices, ASM international (2006).

[5] G. Karthik, B. Kashyap, T.R. Prabhu, Mater. Today-Proc. **4**, 3581-3589 (2017). DOI: https://doi.org/10.1016/j.matpr.2017.02.250

[6] D.C. Lagoudas, Shape memory alloys: modeling and engineering applications,1st ed. New York: Springer (2010).

[7] P.S. Lobo, J. Almeida, L. Guerreiro, Procedia Engineer. **114**, 776-783 (2015). DOI: https://doi.org/10.1016/j.proeng.2015.08.025

[8] J. Frenzel, E.P. George, A. Dlouhy, Ch. Somsen, M.F.X. Wagner, G. Eggeler, Acta Mater. **58**, 3444-3458 (2010). DOI: https://doi.org/10.1016/j.actamat.2010.02.019

[9] D.V. Shtansky, SHS Materials in Medicine, Concise Encyclopedia of Self-Propagating High-Temperature Synthesis, 325-327 (2017).

[10] M.J. Garcia-Ramirez, R. Lopez-Sesenes, I. Rosales-Cadena, J.G. Gonzalez-Rodriguez, J. Mater. Sci. Technol. **7**, 223-230 (2018). DOI: https://doi.org/10.1016/j.jmrt.2017.07.003

[11] B.E. Franco, J. Ma, B. Loveall, G.A. Tapia, K. Karayagiz, J. Liu, A. Elwany, R. Arroyave, I. Karaman, Scientific reports **7.1**, 1-12. (2017). DOI: https://doi.org/10.1038/s41598-017-03499-x

[12] H. Hou, Y. Tang, R.F. Hamilton, M.W. Horn, J. Vac. Sci. Technol. A., **35**, 040601 (2017). DOI: https://doi.org/10.1116/1.4983011

[13] G.D. Travassos, L.F.A. Rodrigues, C.J. de Araújo, J. Braz. Soc. Mech. Sci. **39**, 1269-1275 (2017). DOI: https://doi.org/10.1007/s40430-016-0617-4

[14] N. Duraipandy, K.M. Syamala, N. Rajendran, Appl. Surf. Sci. **427**, 1166-1181 (2018). DOI: https://doi.org/10.1016/j.apsusc.2017.08.221

[15] S. A. Pauline, N. Rajendran, Ceram. Int. **43**, 1731-1739 (2017). DOI: https://doi.org/10.1016/j.ceramint.2016.08.207

[16] I. C. Conceição, L.C.M. Dias, A.M. Fernandes, R.L.P. Teixeira, F. Moura, H.L. Hasegawa, J.C. de Lacerda, J.C.E. C. **3**, 1038-1050 (2017). DOI: https://doi.org/10.18540/jcecv13iss8pp1038-1050

[17] R.L.P. Teixeira, G.C.D. Godoy, M.M. Pereira, Mater. Res-Ibero-Am. J. **7**, 299-303 (2004). DOI: http://dx.doi.org/10.1590/S1516-14392004000200013

[18] NCCLS, Performance Standards for Antimicrobial Disk Susceptibility Tests; Approved Standard-Eighth Edition, NCCLS document M2-A8 [ISBN 1-56238-485-6], USA (2003).

[19] ICDD, PDF 9-432 (Database), Kabekkodu, S., Ed., Newtown Square: Int. Centre Diffraction Data (2010).

[20] C.J. Wilcock, G.P. Stafford, C.A. Miller, Y. Ryabenkova, M. Fatima, P. Gentile, G. Möbus, P.V. Hatton, J. Biomed. Nanotechnol. **13**, 1168-1176 (2017). DOI: https://doi.org/10.1166/jbn.2017.2387

[21] D. Siek, A.D. Ślósarczyk, A. Przekora, A. Belcarz, A. Zima, G. Ginalska, J. Czechowska, Ceram. Int. **43**, 13997-14007 (2017). DOI: https://doi.org/10.1016/j.ceramint.2017.07.131

[22] International standard: Biological Evaluation of Medical Devices Part 5: Tests for Cytotoxicity: in vitro methods. ISO 10993-5 (2009).

[23] C. de Souza, R.L.P. Teixeira, J.C. de Lacerda, C.R. Ferreira, C.H.S.B. Teixeira, V.T. Signoretti. Polímeros **28.3**, 226-230 (2018). DOI: https://dx.doi.org/10.1590/0104-1428.015816

[24] J. Málek, F. Hnilica, J. Veselý, B. Smola, R. Medlín, J. Mech. Behav. Biomed. **75**, 252-261 (2017). DOI: https: //doi.org/10.1016/j.jmbbm.2017.07.032

[25] T.W. Duerig, A.R. Pelton, Ti-Ni shape memory alloys, Materials Properties Handbook, Titanium Alloys, Materials Park. OH: American Society for Metals, 1035-1048 (1994)

[26] G. Karthik, B. Kashyap, T.R. Prabhu, Mater. Today-Proc. **4**, 3581-3589 (2017). DOI: https://doi.org/10.1016/j.matpr.2017.02.250

[27] M. Iijima, W.A. Brantley, I. Kawashima, H. Ohno, W. Guo, Y. Yonekura, I. Mizoguchi, Biomaterials **25**, 171-176 (2004). DOI: https://doi.org/10.1016/S0142-9612(03)00473-3

[28] T.A. Thayer, M.D. Bagby, R.N. Moore, R.J. DeAngelis, Am. J. Orthod. Dentofac. **107**, 604-612 (1995). DOI: https://doi.org/10.1016/S0889-5406(95)70103-6.

[29] B.L. Pereira, C.M. Lepienski, I. Mazzaro, N.K. Kuromoto, Mater. Sci. Eng. C. **77**, 1235-1241 (2017). DOI: https://doi.org/10.1016/j.msec.2016.10.073

[30] K.K. Carneiro, T.P. Araujo, E.M. Carvalho, M.M. Meier, A. Tanaka, C.N. Carvalho, J. Bauer, J. Mech. Behav. Biomed. **78**, 188-195 (2018). DOI: https://doi.org/10.1016/j.jmbbm.2017.11.016

[31] M. Tamai, K. Isama, R. Nakaoka, T. Tsuchiya, J. Artif. Organs. **10**, 22-28 (2007). DOI: https://doi.org/10.1007/s10047-006-0363-y

[32] P.W. Brown, B. Constantz, Hydroxyapatite and related materials, CRC press (2017).

[33] S. Raynaud, E. Champion, D. Bernache-Assollant, P. Thomas, Biomaterials **23**, 1065-1072 (2002). DOI: https://doi.org/10.1016/S0142-9612(01)00218-6